RAA 2021 Vol. **21** No. **11**, 270(9pp) doi: 10.1088/1674-4527/ac2943

http://www.raa-journal.org *http://iopscience.iop.org/raa*

***R**esearch in*
***A**stronomy and*
***A**strophysics*

Probing dark contents in globular clusters with timing effects of pulsar acceleration

Li-Chun Wang[1,2] and Yi Xie[1]

[1] School of Science, Jimei University, Xiamen 361021, China; *xieyi@jmu.edu.cn*
[2] Physics Experiment Center, Jimei University, Xiamen 361021, China

Received 2021 August 7; accepted 2021 September 17

Abstract We investigate pulsar timing residuals due to the coupling effect of the pulsar transverse acceleration and the Römer delay. The effect is relatively small and usually negligible. Only for pulsars in globular clusters, it is possibly important. The maximum residual amplitude, which is from the pulsar near the surface of the core of the cluster, is about tens of nanoseconds, and may hardly be identified for most globular clusters currently. However, an intermediate-mass black hole in the center of a cluster can apparently increase the timing residual magnitudes. Particularly for pulsars in the innermost core region, their residual magnitudes may be significant. The high-magnitude residuals, which are above critical lines of each cluster, are strong evidence for the presence of a black hole or dark remnants of comparable total mass in the center of the cluster. We also explored the timing effects of line-of-sight accelerations for the pulsars. The distribution of measured line-of-sight accelerations are simulated with a Monte Carlo method. Two-dimensional Kolmogorov-Smirnov tests are performed to reexamine the consistency of distributions of the simulated and reported data for various values of parameters of the clusters. It is shown that the structure parameters of Terzan 5 can be constrained well by comparing the distribution of measured line-of-sight accelerations with the distributions from Monte Carlo simulations. We find that the cluster has an upper limit on the central black hole/dark remnant mass of $\sim 6000\,M_{\odot}$.

Key words: pulsars: general — globular clusters: general — stars: black holes

1 INTRODUCTION

Intermediate-mass black holes (IMBHs) are black holes (BHs) with mass between $10^2 - 10^5\ M_{\odot}$. They are considered as the missing link between stellar-mass BHs and supermassive BHs (Haiman et al. 2013). Although it has long been suspected that IMBHs may form in the centers of globular clusters (GCs) (Bahcall & Ostriker 1975), the existence of IMBHs in GCs remains in doubt.

Two traditional methods have been widely applied to reveal the IMBHs in GCs. The first is studying the dynamics of the stars through optical observations, by which the past researches inferred upper limits on the mass of the IMBHs (McLaughlin et al. 2006; van der Marel & Anderson 2010; Aros et al. 2020), or made a few tentative detections (Noyola et al. 2008; Lützgendorf et al. 2013). The second is looking for signatures of X-ray and radio emission from the accreting IMBHs (Maccarone 2004). However, some controversial limits on the masses were obtained with this approach (Pooley & Rappaport 2006; de Rijcke et al. 2006; Miller-Jones et al. 2012; Sun et al. 2013; Tremou et al. 2018). Recently, an IMBH in an extragalactic stellar cluster might have been found through the observation of a tidal disruption event (Lin et al. 2018).

Pulsars are very stable rotators, which emit radio pulses to the Earth with regular arrival times. Pulsar timing analysis is based on the measurement of precise times of arrival (TOAs) at the telescope, which provide the spin period and its derivatives of the pulsar. However, many pulsars exhibit significant timing irregularities, i.e., unpredictable TOAs of the pulses, namely timing residuals. Pulsar timing residuals, which widely exist, can be produced by many mechanisms (e.g., Hobbs et al. 2010), one of which especially concerned here is an observed delay, the Römer delay, due to the Earth being at a point in its orbit further from the pulsar as compared to the times when it is at the point nearer the pulsar. Then, a growing sinusoidal pattern of the residuals will be observed if the pulsar has proper motion. This was first achieved for PSR B1133+16 considering a four-year period of observations (Manchester et al. 1974). The coupling effect of the pulsar transverse acceleration $a_{\perp}$ and the Römer delay induces

very similar timing residual patterns, but their oscillation envelopes consist of two parabolic curves, rather than straight lines (Xie & Wang 2020). However, the residuals are usually negligible in timing analysis, since they are relatively small (Edwards et al. 2006), and at present there is no relevant report on them.

GCs are extremely prolific millisecond pulsar (MSP) factories. Observational and theoretical evidences suggest that there are probably more than ~ 1000 MSPs in some massive GCs (Turk & Lorimer 2013). It was anticipated that a pulsar in a dense environment of the host GC would experience varying accelerations due to close encounters with nearby stars, and this effect could act as a probe for the cluster dynamics (Blandford et al. 1987). It was also noticed that the resultant perturbations in acceleration cannot be measured directly using pulsar timing analysis, since they would be absorbed into the pulsar spin parameters of the timing model (Blandford et al. 1987; Phinney 1992). However, due to the motion of a pulsar through the gravitational potential of GCs, the Doppler effect in the line-of-sight direction may overwhelm the intrinsic positive spin period derivative $\dot{P}$; the concept was further developed to study the intrinsic characteristics, structure and components of the GCs (Phinney 1992, 1993). Very recently, new evidences were obtained for the identification of IMBHs, by measuring the effects on accelerations, jerks or jounces of MSPs in GCs (Prager et al. 2017; Freire et al. 2017; Perera et al. 2017; Abbate et al. 2019a,b). Further, the pulsar acceleration measurements together with the dynamical N-body simulations of the cluster provided some striking constraints on the mass of an IMBH in the center of the GC (Kızıltan et al. 2017; Baumgardt 2017; Baumgardt et al. 2019).

However, only the line-of-sight acceleration $a_{\rm l}$ of pulsars is related with the previous measurements for the IMBHs. The effect of transverse acceleration $a_\perp$, which contains complementary information, still received little attention. It was proposed that the magnitudes of the timing residuals due to the coupling effect of $a_\perp$ and the Römer delay may be important for pulsars deposited in the core region of a nearby GC (Xie & Wang 2020). Probably, if an IMBH is present in the center of a GC, $a_\perp$ may be sensitive to the mass of the BH, especially for pulsars in the inner region. Thus, this type of timing residual (due to the coupling effect) may possibly be identified for pulsars in the center region of the GC. In turn, the amplitudes of the residuals may also provide additional constraints on the mass of the central BH.

In this work, we estimate the magnitudes of the residuals for pulsars near the core region of GCs in Section 2, the residuals can be used to probe the mass of IMBHs in the center of GCs, and the structure parameters of Terzan 5 (Ter 5) can be constrained by comparing the distribution of measured $a_{\rm l}$ with the distributions from Monte Carlo simulations, as described in Section 3. Finally, the results are summarized and discussed in Section 4.

2 METHODS

The coupling effect is essentially attributed to the geometric propagation delay. Following the convention of math in timing analysis (Edwards et al. 2006), the displacement $\boldsymbol{k}$ of a pulsar may be broken into its first and second derivatives,

$$\boldsymbol{k} = \boldsymbol{\mu}|\boldsymbol{R_0}|(t^{\rm psr} - t_{\rm pos}) + \frac{\boldsymbol{a}}{2}(t^{\rm psr} - t_{\rm pos})^2, \quad (1)$$

where $\boldsymbol{\mu}$ is the velocity divided by the distance, $\boldsymbol{R_0}$ is the position vector of the pulsar, $\boldsymbol{a}$ is the acceleration vector and $t^{\rm psr}$ is the proper time measured at the pulsar since epoch $t_{\rm pos}$. Substituting the displacement $\boldsymbol{k}$ into the annual proper motion term, i.e., the second term in the first pair of parentheses of equation (5) in Edwards et al. (2006), we have

$$\begin{aligned}\frac{\boldsymbol{k}_\perp \cdot \boldsymbol{r}_\perp}{|\boldsymbol{R_0}|} =& \boldsymbol{\mu}_\perp \cdot \boldsymbol{r}_\perp (t^{\rm psr} - t_{\rm pos}) \\ &+ \frac{\boldsymbol{a}_\perp \cdot \boldsymbol{r}_\perp}{2|\boldsymbol{R_0}|}(t^{\rm psr} - t_{\rm pos})^2,\end{aligned} \quad (2)$$

in which $\boldsymbol{r}$ is the barycentric position of the observatory, the radial and transverse components are denoted by subscripts, i.e., $i_\parallel = \boldsymbol{i}\cdot\boldsymbol{R_0}/|\boldsymbol{R_0}|$ and $\boldsymbol{i}_\perp = \boldsymbol{i} - i_\parallel \boldsymbol{R_0}/|\boldsymbol{R_0}|$, and $\boldsymbol{i}$ is an arbitrary vector. In equation (5) of Edwards et al. (2006), only the first three terms in the first pair of parentheses involve the displacement $\boldsymbol{k}$ of the pulsar. The first term corresponds to the Shklovskii effect, which mainly acts on the line-of-sight acceleration and has no other important effect on the timing residual, is a tiny contribution to the measured acceleration (Prager et al. 2017) and is also small compared to the second term, since $|\mathbf{k}| \ll |\mathbf{r}|$. The third term is ignored, since it is analog ous to the second term, and $|\boldsymbol{b}| \ll |\boldsymbol{r}|$ for almost all the binary pulsars in GCs, where $\boldsymbol{b}$ is the position of the pulsar with respect to the binary barycenter. The absolute values of the second, third and fourth terms in the second pair of parentheses are much smaller than one. Thus only the second term in the first pair of parentheses is considered in this work.

The amplitude of the timing residual due to the coupling effect of the transverse acceleration $\boldsymbol{a}_\perp$ and the Römer delay can be expressed as,

$$\Delta'_{\rm R\odot} = \frac{\boldsymbol{a}_\perp \cdot \boldsymbol{r}_\perp}{2|\boldsymbol{R_0}|c}(t^{\rm psr} - t_{\rm pos})^2, \quad (3)$$

where c is the speed of light.

Due to the Doppler effect, a pulsar with rest frame period P_0 is observed to have a period P (Phinney 1993; Prager et al. 2017),

$$P = [1 + (\mathbf{V}_{\rm p} - \mathbf{V}_{\rm bary}) \cdot \mathbf{n}/c]P_0, \quad (4)$$

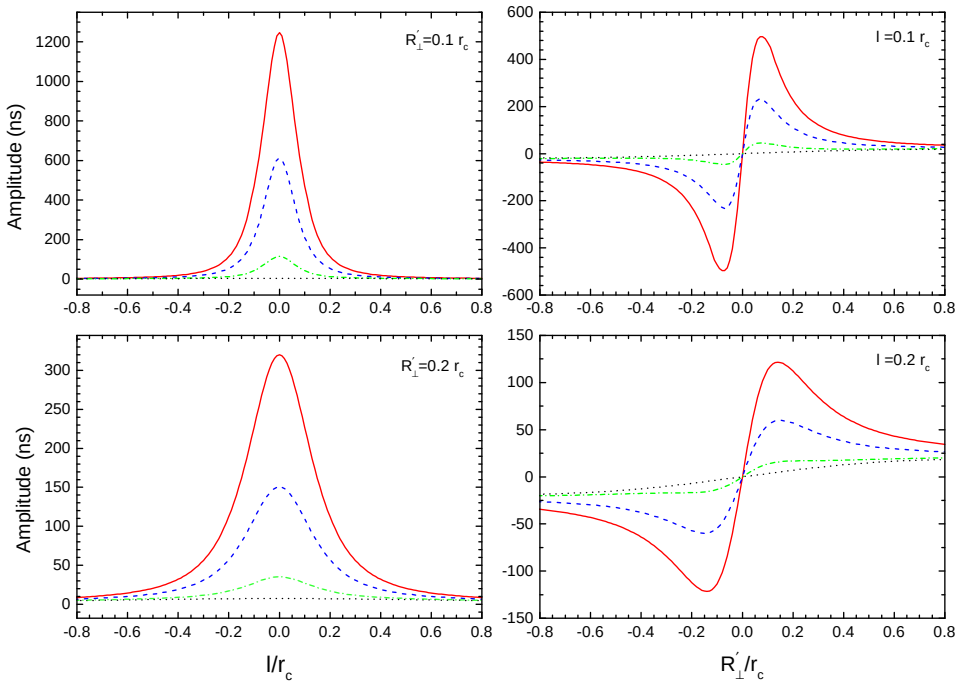

Fig. 1 The amplitudes of timing residuals due to the coupling effect of the pulsar transverse acceleration and the Römer delay, for pulsars in the inner region of a GC with $\rho_c = 10^6\ M_\odot\ \mathrm{pc}^{-3}$ and $r_c = 0.2$ pc, for a 20-yr observing campaign. Left panels: the residual amplitudes with respect to l, $R'_\perp = 0.1r_\mathrm{c}$ (*top panel*) and $0.2r_\mathrm{c}$ (*bottom panel*) are taken in the calculation. Right panels: the amplitudes with respect to $R'_\perp$, $l = 0.1r_\mathrm{c}$ (*top*) and $0.2r_\mathrm{c}$ (*bottom*) are adopted. For all the panels, the *dotted lines*, *dot-dashed lines*, *dashed lines* and *solid lines* represent $m_\mathrm{BH} = 0$, 1000, 5000 and 10 000, respectively.

where $\mathbf{V}_\mathrm{bary}$ is the velocity of the solar system barycenter, $\mathbf{V}_\mathrm{p}$ is the pulsar velocity and $\mathbf{n}$ is the unit vector along the line-of-sight. The time derivative of Equation (4) gives (Prager et al. 2017)

$$\frac{\dot{P}}{P} = \frac{\dot{P}_0}{P_0} + \frac{a_\mathrm{l}}{c} + \frac{a_\mathrm{g}}{c} + \frac{a_\mathrm{s}}{c} + \frac{a_\mathrm{DM}}{c}, \tag{5}$$

in which the pulsar acceleration is decomposed into four terms, a_l is the line-of-sight acceleration due to the GC potential, a_g is the acceleration due to the Galactic potential, a_s is the apparent acceleration from the Shklovskii effect and a_DM is the apparent acceleration due to errors in the changing dispersion measure. a_g, a_s and a_DM are neglected in our model, since they are all much smaller than a_l (Prager et al. 2017).

We now derive the contribution for a pulsar's acceleration that arises due to the GC's mean field and the influence of the IMBH at the center of gravity (CoG)[1]. We define a coordinate system for the GC: the plane passing through the CoG and perpendicular to our line-of-sight is defined as O, the impact parameter for a pulsar from the CoG as $R'_\perp$, and the line-of-sight position going perpendicularly through O as l, and thus the pulsar's spherical radius $r' = \sqrt{R'^2_\perp + l^2}$.

The IMBH for a given mass M_BH has a radius of influence (Baumgardt et al. 2004),

$$r_i = \frac{3M_\mathrm{BH}}{8\pi\rho_c r_c^2}, \tag{6}$$

where ρ_c is the core density of the GC and r_c is the core radius. Within r_i, the gravitational influence of the BH is dominant and the density profile obeys $\rho_\mathrm{BH} \propto r^{-\alpha}$ (Prager et al. 2017). The power index $\alpha = 1.55$ is found through N-body simulations of multiple component masses in the core (Baumgardt et al. 2004). At r_i and beyond, the density profile follows the modified King density profile (Elson profile) as

$$\rho(r') \simeq \rho_\mathrm{c}[1 + (r'/r_\mathrm{c})^2]^{-\frac{\beta}{2}}, \tag{7}$$

in which the power-law slope β is an undetermined parameter. The form of the density profile is widely utilized for star clusters in the Large Magellanic Cloud (Elson 1992) and the model is the same as King's model for $\beta = 3$ (King 1962). Integrating density profiles

[1] It is assumed that the IMBH is fixed to the center of the cluster, and this is most valid for larger BH masses.

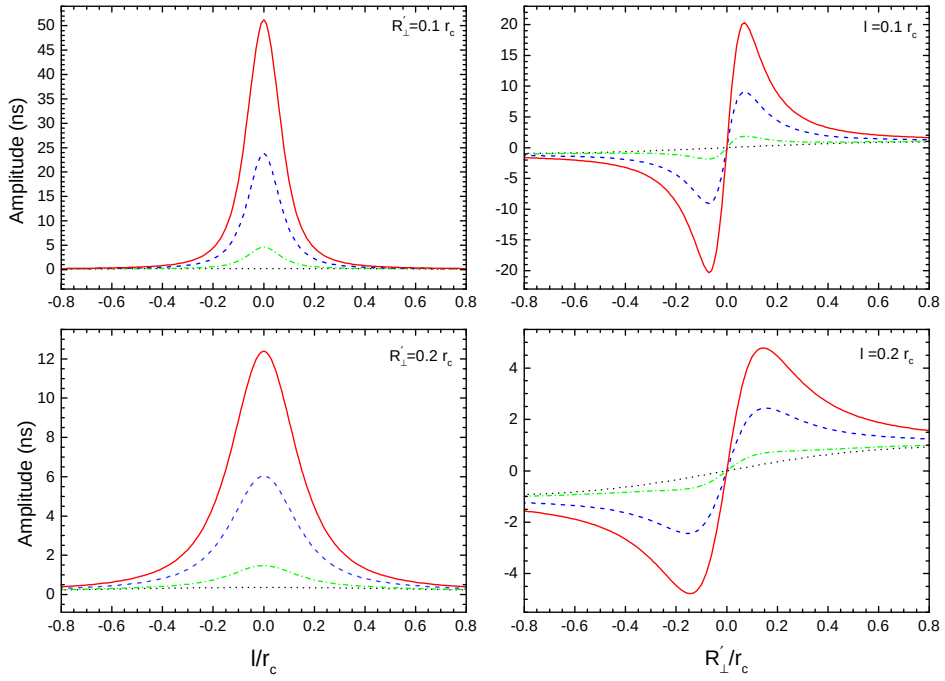

Fig. 2 The same as Fig. 1 but for pulsars in the inner region of a GC with $\rho_c = 10^4\ M_\odot\ \mathrm{pc}^{-3}$ and $r_c = 1.0$ pc.

radially yields the interior mass at any given radius r'_*. The acceleration felt at r'_* can be obtained by multiplying G/r'^2_*, which reads,

$$a(r'_*) = \frac{4\pi G}{r'^2_*}[M_{\rm BH}/4\pi + \int_0^{r_i} r'^2 \rho_{\rm BH} dr' + \int_{r_i}^{r'_*} r'^2 \rho(r') dr']. \quad (8)$$

The $\rho_{\rm BH}$ term contains only the density profile of GC stars under the influence of a central BH. For a radius beyond r_i, the BH has little impact on the density of GC stars. However, the acceleration felt by a pulsar should consider the gravity of the central BH (i.e. the first term in square brackets). One can get the transverse acceleration $a_\perp$ by projecting the acceleration $a(r'_*)$ along the transverse direction by a factor of $R'_\perp/r'_*$, or the line-of-sight acceleration $a_{\rm l}$ by a factor of l/r'_*.

3 APPLICATIONS

3.1 Timing Residuals due to The Coupling Effect

The methods are applicable to all the Galactic GCs. Among them, Ter 5 has the largest number of identified MSPs, which is about a quarter of the total population (39/230) of pulsars in Galactic GCs[2]. The majority lies within the inner 20 arcminutes of the cluster (Prager et al. 2017). It is very suitable to use the basic parameters of Ter 5 as an example for demonstrating the magnitudes of the coupling effect for pulsars distributed around the CoG. Using the accelerations and jerks of the ensemble of Ter 5 MSPs, the core density $\rho_c = 1.58^{+0.13}_{-0.13} \times 10^6\ M_\odot\ \mathrm{pc}^{-3}$ and the core radius $r_c = 0.16^{+0.01}_{-0.01}$ pc were obtained (Prager et al. 2017), and r_c agrees with the values derived from high resolution *Hubble Space Telescope* data (Miocchi et al. 2013). The most accurate distance estimate of the cluster is $d_0 = 5.9 \pm 0.5$ kpc (Valenti et al. 2007), and the value is inversely proportional to the residual amplitudes.

We consider a Ter 5-like cluster with the core density $\rho_c = 10^6\ M_\odot\ \mathrm{pc}^{-3}$ and core radius $r_c = 0.2$ pc, and a typical cluster with $\rho_c = 10^4\ M_\odot\ \mathrm{pc}^{-3}$, $r_c = 1.0$ pc and $d_0 = 10$ kpc is taken for both types in the following calculations. We consider an IMBH with mass of $m_{\rm BH}$, expressed in $M_\odot$, in the center of the cluster. Combining Equations (3), (6)–(8) and substituting the cluster parameters, one can obtain the amplitudes of the residuals for various l or $R'_\perp$. As examples, we display the residual amplitudes for pulsars in the Ter 5-like cluster in Figure 1. The left panels are the amplitudes with respect to l with $R'_\perp = 0.1r_{\rm c}$ (top panel) and $0.2r_{\rm c}$ (bottom panel). The right panels are the amplitudes with respect to $R'_\perp$ with $l = 0.1r_{\rm c}$ (top) and $0.2r_{\rm c}$ (bottom). For all

[2] http://www.naic.edu/~pfreire/GCpsr.html

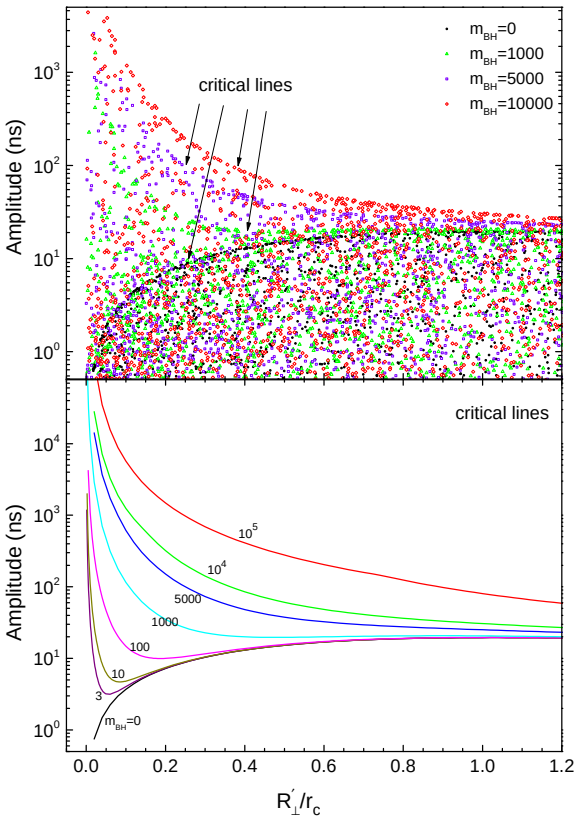

Fig. 3 *Top*: the simulated distributions of residual amplitudes due to the coupling effect of the pulsar transverse acceleration and the Römer delay, for pulsars in the inner region of a GC with $\rho_c = 10^6\ M_\odot\,\mathrm{pc}^{-3}$ and $r_c = 0.2$ pc, for a 20-yr observing campaign. The *black points*, *green triangles*, *blue squares* and *red diamonds* represent $m_{\rm BH} = 0$, 1000, 5000 and 10 000, respectively. *Bottom*: the critical lines of the distributions (from the maximum value fitting) for $m_{\rm BH} = 0$, 3, 10, 100, 1000, 5000, 10^4 and 10^5, respectively.

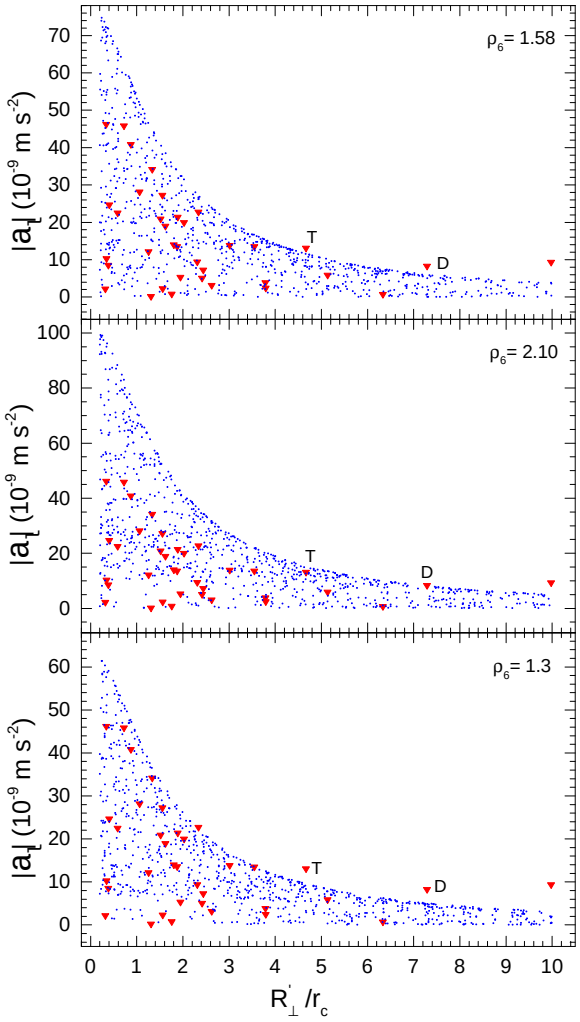

Fig. 4 The simulated $a_{\rm l}$ distributions for pulsars in Ter 5. The *red triangles* represent the measured $a_{\rm l}$ values and the *blue points* are the simulated $a_{\rm l}$ values. The upper panel, middle panel and lower panel depict the simulations for $\rho_6 = 1.58$, 2.1 and 1.3, respectively. For all the simulated results, $r_c = 0.16$ pc and $\beta = 3$ are taken.

the panels, the dotted lines, dot-dashed lines, dashed lines and solid lines correspond to $m_{\rm BH} = 0$, 1000, 5000 and 10 000, respectively. The results imply that if there is an IMBH, the residuals due to the coupling effect may have some chance to be identified, particularly for those pulsars that are distributed in the vicinity of the CoG and near the O plane. We also calculated the case of no IMBH in the center. The maximum amplitude is from the pulsar at the surface of the core, which is about 20 ns. This amplitude is relatively small, even for those pulsars with the highest timing precision (Perera et al. 2019). Figure 2 features the residual amplitudes for pulsars in the inner region of a typical cluster with $\rho_c = 10^4\ M_\odot\,\mathrm{pc}^{-3}$ and $r_c = 1.0$ pc. The amplitudes are below 50 ns for all the cases of $m_{\rm BH} \lesssim 10^4$ for pulsars beyond 0.1 r_c, and thus hardly can be observed currently. Cross calculations indicate that the amplitude differences between the Ter 5-like cluster and the typical cluster are mainly due to the distance r'_* from the pulsar to the CoG, as well as the projection distance $R'_\perp$, since at the innermost region of the clusters, the residuals are dominated by the effects of gravity from the IMBHs (if they are present), where the total mass of the interior stars M_* is less than the mass of the IMBH in each cluster, e.g., $M_* < 100\ M_\odot$ for $r'_* < 0.2 r_{\rm c}$ for both of the types of clusters.

For a complete profile of the residual magnitudes in the parameter space, we perform Monte Carlo (MC) simulations on the pulsar distribution in the core region of the cluster. In the simulations, the column number density profile of the pulsars is assumed to obey the following

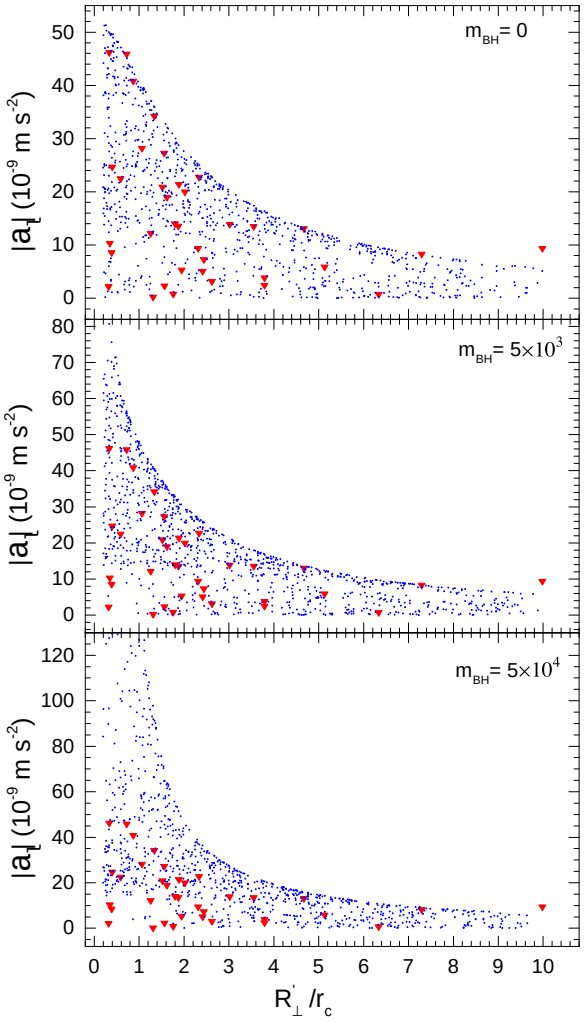

Fig. 5 The simulated $a_{\rm l}$ distributions for pulsars in Ter 5. The *red triangles* represent the measured $a_{\rm l}$ values, and the *blue points* are the simulated $a_{\rm l}$ values. The upper panel, middle panel and lower panel depict the simulations for $m_{\rm BH} = 0$, 5×10^3 and 5×10^4, respectively. For all the simulated results, $\rho_c = 0.95 \times 10^6\, M_\odot\, {\rm pc}^{-3}$, $r_c = 0.16\,{\rm pc}$ and $\beta = 2.4$ are taken.

formula (Lugger et al. 1995)

$$n(x_\perp) = n_0 (1 + x_\perp^2)^{q/2}, \tag{9}$$

where n_0 is the central number density, $x_\perp \equiv R'_\perp / r_c$ is the distance from the center in the plane of the sky in units of the core radius and $0 < x \leq 10$ is taken in the following simulations. q is the mass segregation parameter, we take the prior on this parameter to be a Gaussian centered on -3 with a dispersion of 0.5 (Abbate et al. 2019b). The mass interior to the radial position of each pulsar is calculated for the acceleration in simulations. Since the nearest neighbor stars present a negligible contribution to the line-of-sight acceleration (Prager et al. 2017), we propose that the transverse accelerations from the nearest neighbor stars are also smaller than that from the total interior mass. On the other hand, the residual patterns of the errors in the line-of-sight accelerations are apparently different from the patterns of the coupling effect. Thus their contributions to the residuals are also ignored, and only the residuals due to the coupling effect of the transverse acceleration from the total interior mass and the Römer delay are concerned here.

The comparisons between the simulated results with the different masses of the central BHs are depicted in the top panel of Figure 3, for the Ter 5-like cluster, whose pulsar residuals could be very significant. The results for $m_{\rm BH} = 0$, 1000, 5000 and 10^4 are represented by the black points, green triangles, blue squares and red diamonds, respectively. The simulations agree with the results of Figure 1. Different from the case of $m_{\rm BH} = 0$, the presence of an IMBH in the center strongly affects the residual magnitudes of pulsars around it. The residuals of some pulsars at the innermost region ($x_\perp \lesssim 0.4$) may be rather significant, and the root mean square of the residuals due to the effect may be higher than 1 μs. Up-to-date, the reported nearest pulsar from the center of Ter 5 on the plane of the sky is J1748 − 2446I, whose projected separation is about $0.3 r_c$. The results imply that the high-magnitude residuals due to the coupling effect may have the chance to be identified for pulsars in the innermost region of GCs.

It is noteworthy that the residual amplitudes cannot be higher than the upper boundary line for $m_{\rm BH} = 0$, unless an IMBH is present. Thus the observations of pulsars with high-magnitude residuals will strongly support the existence of an IMBH in the center. The upper boundary line can actually play the role of a critical line for BH identification for each cluster. The critical lines can also be fitted with the maximum values of the simulated amplitudes, for different values of $m_{\rm BH}$. As plotted in the bottom panel of Figure 3, a pulsar with residual amplitude higher than a critical line indicates the presence of a BH with mass higher than the corresponding value of the line. Because of symmetry, we only show the region $R'/r_c \geqslant 0$ in Figure 3, corresponding to the right half of the right panels of Figures 1 and 2. In the right panels of Figures 1 and 2, the amplitude at $R'/r_c = 0$ is exactly zero for a fixed l, and the peak values are larger and going to be close to $R'/r_c = 0$ for a smaller l. Therefore, the critical lines, which are actually formed by all the maximum points of the amplitude lines for various values of l, approach infinity when l and R' approach zero if an IMBH is present.

3.2 GC Parameter Fits Using $a_{\rm l}$ Data

For an investigation of the structure parameters of Ter 5, we perform Monte Carlo simulations on $a_{\rm l}$ distributions of

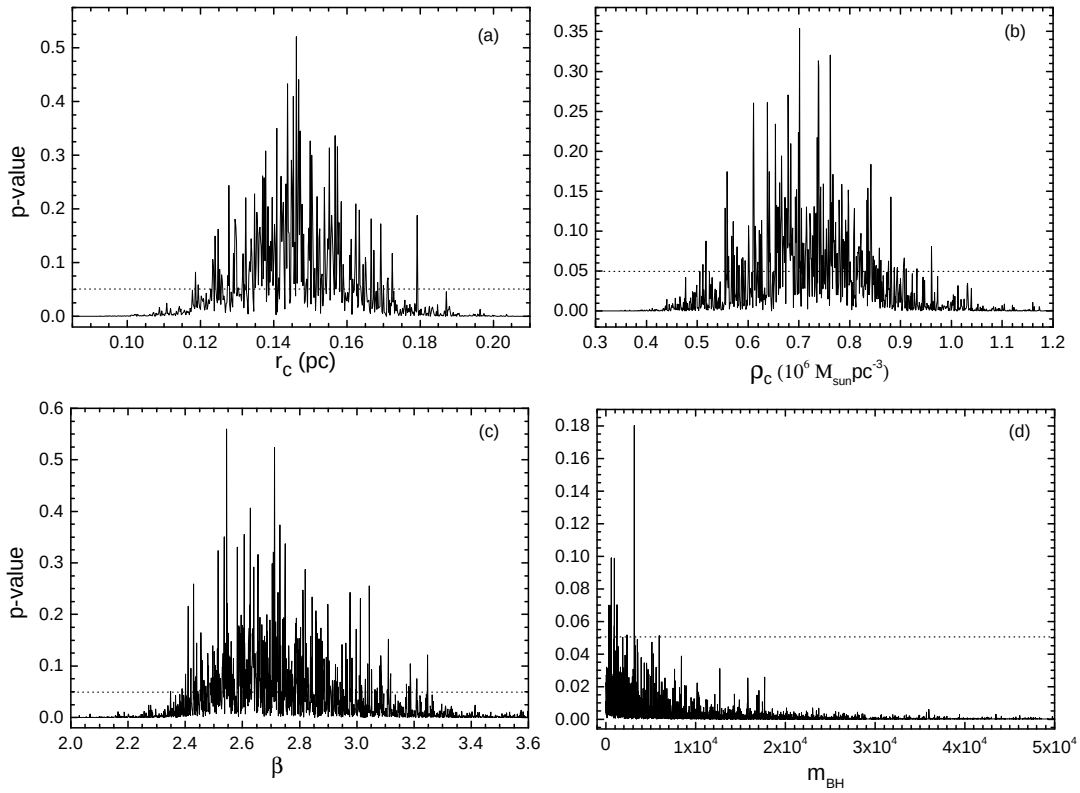

Fig. 6 The p-values of 2DKS for $R_\perp - a_\mathrm{l}$ distributions from the comparisons of measured data with simulated data. The ranges of p-values larger than 0.05 are identified by the transverse lines. Panel (a): for various values of r_c. In the simulations, $\rho_6 = 0.95$, $\beta = 2.4$ and $m_\mathrm{BH} = 0$ are taken. Panel (b): for various values of ρ_c. In the simulations, $r_\mathrm{c} = 0.16$ pc, $\beta = 2.4$ and $m_\mathrm{BH} = 0$ are adopted. Panel (c): for various values of β. In the simulations, $r_\mathrm{c} = 0.16$ pc, $\rho_6 = 0.95$ and $m_\mathrm{BH} = 0$ are taken. Panel (d): for various values of m_BH. In the simulations, $r_\mathrm{c} = 0.16$ pc, $\rho_6 = 0.95$ and $\beta = 2.4$ are adopted.

pulsars in the inner region of the cluster with Equations (5)–(9). The timing parameters for Ter 5 pulsars are taken from table 1 and the data of $R_\perp$ are referenced from table 4 of Prager et al. (2017). For convenience, we assume $\rho_6 = \rho_c/10^6\ M_\odot\,\mathrm{pc}^{-3}$. The simulated distributions are displayed in Figure 4. *There are only a few pulsars with maximum acceleration values that provide the strongest constraints for GC structure parameters. A precondition is assumed in the simulations that the area of the measured data should be covered well by the simulated data.* One can see that there are two pulsars, J1748-2446T and J1748-2446D, which cannot be covered well with simulated data for the parameter $\rho_6 = 1.58$, as shown in the top panel. The coverage for the two pulsars needs $\rho_6 \gtrsim 2.1$, as depicted in the middle panel. However the coverage is excessive for the inner part for this case. The optimum coverage of the inner part requires $\rho_6 \sim 1.3$, but the two pulsars cannot be covered either, as demonstrated in the bottom panel.

In order to obtain the best-fit profile and turn measured a_l into a probe of the cluster potential, we substitute Equation (7) into Equation (8) in the following calculations. We found that the simulated distribution with the parameters $\rho_c = 0.95 \times 10^6\ M_\odot\,\mathrm{pc}^{-3}$, $r_c = 0.16$ pc, $m_\mathrm{BH} = 0$ and $\beta = 2.4$ matches the measured data very well, as affirmed in the upper panel of Figure 5. Simulations for $m_\mathrm{BH} = 5 \times 10^3$ and $m_\mathrm{BH} = 5 \times 10^4$ are also featured in the middle and bottom panels, respectively. One can see that the IMBH can dramatically change the distributions of the innermost region.

It is very important to explore the parameter space of the simulations. We perform a two-dimensional Kolmogorov-Smirnov (2DKS) test to reexamine the consistency of distributions of the simulated and measured a_l for series values of the parameters under test. Our strategy is then to search for the values of the parameters that can maximize the p-value of the 2DKS test against the hypothesis that the two distributions are consistent (Xie & Zhang 2019). We firstly let r_c vary from 0.08 pc to 0.21 pc with step size of 2×10^{-4} pc. We draw 200 data points for each test, and the returned p-values are marked with solid lines in panel (a) of Figure 6. The p-value 0.05, which is indicated by a dotted line, is considered as the threshold

level with probability 95%. The test affirms that $0.12\,\mathrm{pc} \lesssim r_c \lesssim 0.19\,\mathrm{pc}$. Similarly, the constraints on the parameters, $0.5 \lesssim \rho_6 \lesssim 1.0$ (testing from 0.3 to 1.2 with a step size of 10^{-3}) and $2.4 \lesssim \beta \lesssim 3.2$ (testing from 2.0 to 3.6 with a step size of 10^{-3}), are also obtained, and the results of p-values are displayed in panels (b) and (c) of Figure 6, respectively. Considering the coverage condition, a tighter restriction on core density and β can be made, $0.9 \lesssim \rho_6 \lesssim 1.0$ and $2.4 \lesssim \beta \lesssim 2.6$. We find good agreement with the result of Prager et al. (2017) for r_c, however, for ρ_c, there is an obvious difference. The main reason for the difference is probably the approximation of equation (27) of Prager et al. (2017), since the obtained values of $a_{\mathrm{l,max}}$ with the equation (e.g. $a_{\mathrm{l,max}} \simeq 165\,(10^{-9}\,\mathrm{m\,m^{-2}})$ for $R'/r_c = 1$, $r_c = 0.16\,\mathrm{pc}$ and $\rho_6 = 1.67$) are apparently larger than the reported data shown in Figures 4 and 5 of the manuscript. It is also noticed that the equation is actually different from equation (3.5) of Phinney (1993). Unfortunately, a direct comparison with the latter is currently unavailable, as few values of velocity dispersion σ have been reported in the region of $R'/r_c < 10$ for the cluster[3]. Finally, we set m_{BH} to vary from 0 to 5×10^4 with a step size of 5, and $0 < m_{\mathrm{BH}} \lesssim 6000$ is obtained. The results of p-values are plotted in panel (d), which provide an upper limit for the mass of a possible IMBH at the core of the cluster. The mass segregation parameter q is also tested. However, it is found that the method cannot place an effective restriction on q.

4 DISCUSSIONS AND CONCLUSIONS

Pulsar timing residuals due to the coupling effect of the pulsar transverse acceleration and the Römer delay are usually negligible. For pulsars in the Galactic field, the acceleration due to the Galactic potential is of the order about $10^{-10}\,\mathrm{m\,s^{-2}}$, which induces timing residual < 1 ns. Only for these pulsars in GCs, this effect is possibly needed. If there is no IMBH in the center, the maximum amplitude gained from pulsars near surface of the core is about tens of ns in a Ter 5-like GC, which thus can hardly be identified currently. However, an IMBH in the center can apparently increase the residual magnitudes of pulsars in the core region. The residuals of pulsars in the innermost region of GCs may be significant. The high-magnitude residuals, above the critical lines of each cluster, are strong evidences for an IMBH in the center. The timing effects of line-of-sight accelerations are also explored. The distributions of measured line-of-sight acceleration versus the projection radius are simulated with the MC method. The 2DKS tests are applied to reexamine the consistency of distributions of the simulated and reported data for various values of parameters of the clusters. We found that the structure parameters of Ter 5 can be constrained well by comparing the distributions of measured a_{l} with MC simulations. It is shown that Ter 5 has an upper limit on the central BH mass of $M_{\mathrm{BH}} \simeq 6000\,M_\odot$. In the work, the same pulsar data from Prager et al. (2017) are used and a tighter constraint on IMBH mass ($\lesssim 6000\,M_\odot$ compared to $\lesssim 30\,000\,M_\odot$) is obtained. However, an intensive analysis for the improvement is still difficult to complete due to the complexity of the statistical processes.

Compared with the Doppler effect (including the line-of-sight accelerations, jerks and jounces), the residual from the coupling effect of the transverse acceleration and the Röemer delay is relatively small, and has not been detected utilizing pulsar timing, and thus cannot provide tighter constraints on the masses of IMBHs currently. However, the residual, whose magnitude is proportional to the observational time span can probably be detected for pulsars in the innermost core region of GCs (see Fig. 3 of the manuscript) in the near future. For a measured acceleration a_l, there are two possible line-of-sight positions (l_1 and l_2) that give the same acceleration, which causes great uncertainty in the parameter determinations. Using the sign of a spin period derivative, one still cannot determine which of the two positions the pulsar is at, since they are on the same side of the pulsar, as shown in figure 1 of Prager et al. (2017). However, the residual from the coupling effect can provide additional information, i.e. constraints from the transverse component of the accelerations $a_\perp$, which may greatly reduce the uncertainty.

Many studies indicate that stellar mass BHs could be common in the centers of GCs (Breen & Heggie 2013; Arca Sedda et al. 2018; Hénault-Brunet et al. 2020). A group of stellar mass BHs with total mass comparable to a single IMBH may have similar effects on pulsar timing and accelerations. One may expect that the two values of β that are obtained from the surface brightness profiles or measured with pulsar accelerations should be the same for a single IMBH in the center. However, for the case of a population of stellar mass BHs (or other dark remnants), the two values of β may be apparently different in the central region of the GCs. Unfortunately, the current analysis cannot unambiguously discriminate between an IMBH and a group of stellar mass BHs of comparable total mass.

We might expect some discoveries of pulsars with high-magnitude residuals in the future, as a good number of MSPs in GCs are reported and being timed regularly. We also expect to gain more details on the residuals and a deeper understanding of GC dynamics, using future larger samples of MSPs with higher precision data, to be facilitated by China's Five-hundred-meter Aperture

[3] https://people.smp.uq.edu.au/HolgerBaumgardt/globular/

Spherical radio-Telescope (FAST) and the future Square Kilometre Array (SKA).

Acknowledgements The anonymous referee is thanked for valuable comments and suggestions which helped to clarify several important points in the revised manuscript. This work is supported by the National Natural Science Foundation of China (Grant Nos. 11803009 and 11603009), and by the Natural Science Foundation of Fujian Province (Grant Nos. 2018J05006, 2018J01416 and 2016J05013).

Note added in proof. After the acceptance of this article for publication, we became aware that pulsar timings and stellar accelerations, used as probes of the Galactic potential and plane mass density, as well as dark matter distribution, have attracted much attention recently (Phillips et al. 2021; Ravi et al. 2019; Chakrabarti et al. 2021; Silverwood & Easther 2019; Buschmann et al. 2021). Using orbital periods of binary pulsars, Phillips et al. (2021) measured the Galactic acceleration with sensitivity in agreement (1σ precision) with the nominal value from the Galactic rotation curve. Ravi et al. (2019) proposed using precision measurement tools developed for exoplanet science to be used to probe stellar accelerations and dark matter distribution in the Galaxy. These works are closely related to this paper.

References

Abbate, F., Spera, M., & Colpi, M. 2019a, MNRAS, 487, 769
Abbate, F., Possenti, A., Colpi, M., et al. 2019b, ApJL, 884, L9
Arca Sedda, M., Askar, A., & Giersz, M. 2018, MNRAS, 479, 4652
Aros, F. I., Sippel, A. C., Mastrobuono-Battisti, A., et al. 2020, MNRAS, 499, 4646
Bahcall, J. N. & Ostriker, J. P. 1975, Nature, 256, 23
Baumgardt, H., Makino, J., & Ebisuzaki, T. 2004, ApJ, 613, 1143
Baumgardt, H. 2017, MNRAS, 464, 2174
Baumgardt, H., He, C., Sweet, S. M., et al. 2019, MNRAS, 488, 5340
Blandford, R. D., Romani, R. W., & Applegate, J. H. 1987, MNRAS, 225, 51P
Breen, P. G. & Heggie, D. C. 2013, MNRAS, 432, 2779
Buschmann, M., Safdi, B. R., & Schutz, K. 2021, arXiv:2103.05000
Chakrabarti, S., Chang, P., Lam, M. T., et al. 2021, ApJL, 907, L26
de Rijcke, S., Buyle, P., & Dejonghe, H. 2006, MNRAS, 368, L43
Edwards, R. T., Hobbs, G. B., & Manchester, R. N. 2006, MNRAS, 372, 1549
Elson, R. A. W. 1992, MNRAS, 256, 515
Freire, P. C. C., Ridolfi, A., Kramer, M., et al. 2017, MNRAS, 471, 857
Haiman, Z., Tanaka, T., Fernandez, R., et al. 2013, SnowPAC 2013 - Black Hole Fingerprints: Dynamics, Disruptions and Demographics, 2
Hénault-Brunet, V., Gieles, M., Strader, J., et al. 2020, MNRAS, 491, 113
Hobbs, G., Lyne, A. G., & Kramer, M. 2010, MNRAS, 402, 1027
King, I. 1962, AJ, 67, 471
Kızıltan, B., Baumgardt, H., & Loeb, A. 2017, Nature, 542, 203
Lin, D., Strader, J., Carrasco, E. R., et al. 2018, MNRAS, 474, 3000
Lugger, P. M., Cohn, H. N., & Grindlay, J. E. 1995, ApJ, 439, 191
Lützgendorf, N., Kissler-Patig, M., Gebhardt, K., et al. 2013, A&A, 552, A49
Maccarone, T. J. 2004, MNRAS, 351, 1049
Manchester, R. N., Taylor, J. H., & Van, Y. Y. 1974, ApJL, 189, L119
McLaughlin, D. E., Anderson, J., Meylan, G., et al. 2006, ApJS, 166, 249
Miller-Jones, J. C. A., Wrobel, J. M., Sivakoff, G. R., et al. 2012, ApJL, 755, L1
Miocchi, P., Lanzoni, B., Ferraro, F. R., et al. 2013, ApJ, 774, 151
Noyola, E., Gebhardt, K., & Bergmann, M. 2008, ApJ, 676, 1008
Perera, B. B. P., DeCesar, M. E., Demorest, P. B., et al. 2019, MNRAS, 490, 4666
Perera, B. B. P., Stappers, B. W., Lyne, A. G., et al. 2017, MNRAS, 468, 2114
Phillips, D. F., Ravi, A., Ebadi, R., et al. 2021, Phys. Rev. Lett., 126, 141103
Phinney, E. S. 1992, Pulsars as Probes of Newtonian Dynamical Systems. Philosophical Transactions of the Royal Society of London Series A 341, 39
Phinney, E. S. 1993, Structure and Dynamics of Globular Clusters, 50, 141
Pooley, D., & Rappaport, S. 2006, ApJL, 644, L45
Prager, B. J., Ransom, S. M., Freire, P. C. C., et al. 2017, ApJ, 845, 148
Ravi, A., Langellier, N., Phillips, D. F., et al. 2019, Phys. Rev. Lett., 123, 091101
Silverwood, H. & Easther, R. 2019, PASA, 36, e038
Sun, M.-Y., Jin, Y.-L., Gu, W.-M., et al. 2013, ApJ, 776, 118
Tremou, E., Strader, J., Chomiuk, L., et al. 2018, ApJ, 862, 16
Turk, P. J. & Lorimer, D. R. 2013, MNRAS, 436, 3720
Valenti, E., Ferraro, F. R., & Origlia, L. 2007, AJ, 133, 1287
van der Marel, R. P. & Anderson, J. 2010, ApJ, 710, 1063
Xie, Y., & Zhang, S.-N. 2019, ApJ, 880, 123
Xie, Y., & Wang, L.-C. 2020, RAA (Research in Astronomy and Astrophysics), 20, 191